Article

Separation Reliability Analysis for the Low-Shock Separation Nut with Mechanism Motion Failure Mode

Lei Niu [1], Hongmao Tu [2], Haiping Dong [1],* and Nan Yan [1]

[1] State Key Laboratory of Explosion Science and Technology, Beijing Institute of Technology, Beijing 100081, China; leiniu1993@163.com (L.N.); yn@bit.edu.cn (N.Y.)

[2] Ordnance Science and Research Academy of China, Beijing 100089, China; bjthm@126.com

* Correspondence: dhpphd@bit.edu.cn

Abstract: A functional reliability simulation method based on the Kriging model is proposed to efficiently evaluate the functional reliability of low-shock separation nuts. First, a deterministic separation function simulation model of the separation nut is established. Second, the working load, geometric dimensions and propellant combustion parameters are introduced to establish the nonlinear implicit function of the separation nut in different separation stages, and the Kriging model is used to display the function. Finally, the functional reliability simulation workflow of the separation nut is established, and reliability and sensitivity analyses are performed to quantify the importance ranking of the working load, geometric size and propellant combustion parameters. It is shown that the influence of the uncertainties can be precisely described, and the preload and the support angle between the piston and nut flap play a dominant role in the separation reliability. This can further support the detailed design of the separation nut.

Keywords: reliability analysis; sensitivity analysis; Kriging model; low-shock separation nut; combustion

1. Introduction

A low-shock separation nut is a type of separation device based on the concept of 'strong connection and soft unlocking', which is widely used in aerospace fields such as fairing separation, rocket stage separation and satellite release. It has the advantages of strong connection capability, low unlocking pressure and low separation shock [1–4]. In recent years, many studies on separation nuts have been conducted by researchers worldwide. Wang et al. [5] used ANSYS AUTODYN to predict the shock response of the separation nut and studied the effects of the preload level and the amount of explosives on the pyroshock response. The simulation results showed that a lower preload is better for reducing pyroshock. Zhao et al. [6] established a finite element model of the separation nut and simulated the separation process of the mechanism based on the finite element analysis method; this revealed the mechanism of the separation shock and provided reference value for designing the separation nut. Woo et al. [7] proposed a mathematical model to predict the complicated coupling behaviour of pyroshock-reduced separation nuts; it contained two variable-volume chambers connected by a vent hole. The model was used to conduct parametric studies for investigating the effects of the design parameters on the separation behaviour. Zhang et al. [8] simulated the dynamic shock process of separation nuts and obtained the load curve at the interface between the satellite and launcher. Lee et al. [9,10] introduced the mechanism of ridge-cut explosive bolts, simulated the work process using ANSYS AUTODYN and conducted a parametric study on specific geometrical dimensions. The simulation analysis of the separation nut in the aforementioned studies was conducted to mainly investigate the function and performance of the separation nut based on factors such as its structure, material and geometric size. A reliability simulation analysis of the separation reliability of the separation nut mechanism has not been performed in literature to the best of the authors' knowledge. The influence of uncertain factors such as the external

load, material properties, structural size and machining error on the separation reliability of the separation nut mechanism has not been considered. Owing to the increasing application of separation nuts in the field of aerospace, the reliability requirements are increasing. It is necessary to conduct a separation reliability analysis of the separation nut mechanism to understand the influence of the external load, material properties, structural size, machining error and other factors on its separation reliability, and appropriate design measures should be proposed to improve the separation reliability level.

The separation reliability analysis of the separation nut mechanism is an implicit function problem. Researchers have proposed many methods to improve the computational efficiency in solving this problem. The surrogate model is mainly used to establish a response model to improve the efficiency of reliability analysis, and it is widely used [11]. Commonly used surrogate models include response surfaces [12,13], support vector machines [14,15], neural networks [16,17] and the Kriging model [18–20]. The response surface method, which is applied to the reliability analysis of implicit functions, is only applicable to low nonlinear functions [21]. For highly nonlinear implicit function problems, support vector machines and neural networks show excellent performance, but their efficiencies are lower than that of the Kriging surrogate model [22]. The Kriging surrogate model is an unbiased estimation model of minimum variance and is characterised by a combination of global approximation and local random error for solving the nonlinear implicit limit state equations of complex mechanisms. Its validity is independent of the existence of random errors, and it has a good fitting effect for the problems of high nonlinearity and sudden changes in the local response. The Kriging surrogate model is used for global and local approximations [23–27]. For these reasons, this paper proposes a functional reliability simulation method for separation nut using the Kriging model.

The remainder of this paper is organised as follows. In Section 1, the research background is introduced. In Section 2, the working principle of the separation nut is introduced, the simulation model of the mechanism separation is described and experimental verification of the accuracy of the simulation model is presented. In Section 3, the reliability model of mechanism separation is detailed based on the nonlinear implicit function of different separation stages of the separation nut. In Section 4, the simulation flow of the separation reliability of the separation nut mechanism is presented. Finally, the conclusions are provided in Section 5.

2. Separation Simulation Model of the Separation Nut Mechanism

2.1. Basic Structure and Working Principle

The structure of a low-shock separation nut is shown in Figure 1. The separating and unlocking mechanisms include the body, inner sleeve, piston, shear pin, nut flap, sealing ring, end cap and other parts.

The separation of the internal mechanisms driven by the propellant gas changes the cavity volume, which affects the cavity pressure and propellant combustion. Based on the relative position of the internal mechanism separation, the mechanism separation state can be divided into the inner sleeve separation stage and the nut flap separation stage, as shown in Figure 2.

During the inner sleeve separation stage, the initiator is ignited, and the gaseous products of gunpowder combustion form pressure in the cavity, driving the inner sleeve to separate and shear the shear pin.

During the nut flap separation stage, when the inner sleeve is separated into a certain stroke, the constraint on the nut flap is released and the nut flap begins to expand radially under the dual action of piston push and bolt preload. When the nut flap expands to a certain distance, the screw teeth of the nut flap are separated from those of the bolt, the constraint of the nut flap on the bolt is released and the bolt flies out under the action of the preload. This completes the separation process.
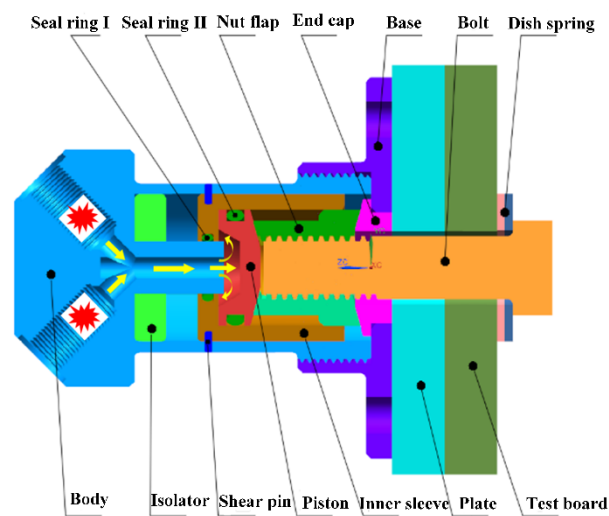
Figure 1. Cross section of low-shock separation nut.
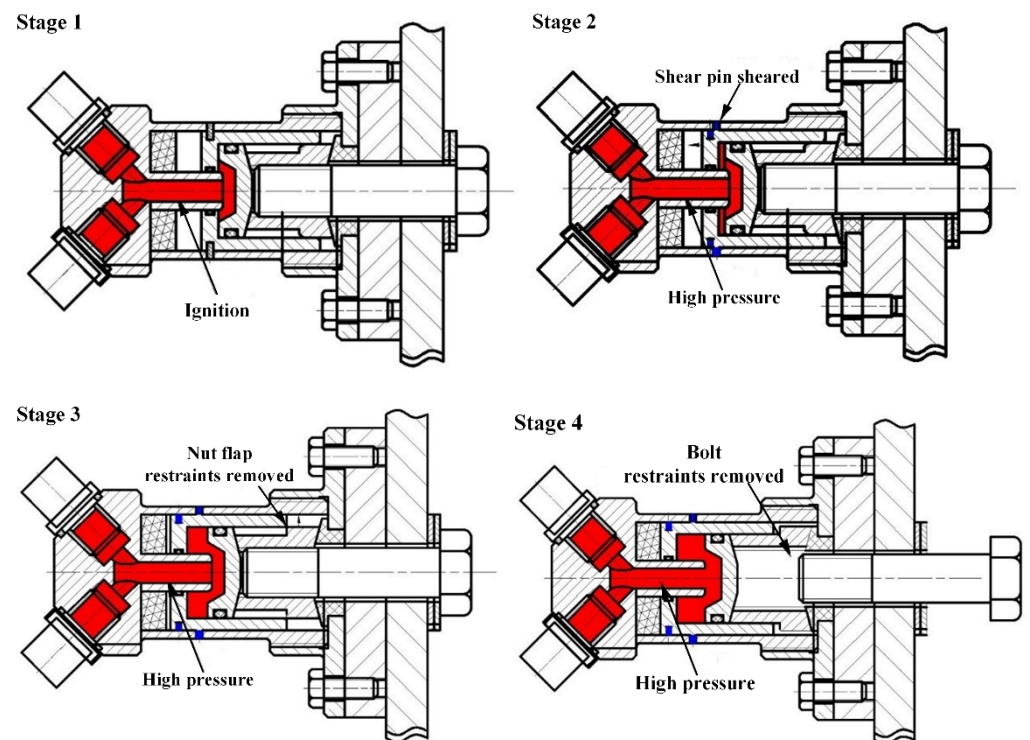
Figure 2. Two key stages of separation nuts mechanism.

2.1.1. Combustion Model

The initiator requires carbon black-potassium nitrate (CPN) as the main explosive charge. This charge consists of numerous minute granules and a binder mixture. The granules have an uneven surface. To simplify the combustion model, the combustion equation is constructed using Equations (1) and (2) [28].

$$\psi = \chi Z(1 + \lambda Z + \mu Z^2) \tag{1}$$

$$\sigma = 1 + 2\lambda Z + 3\mu Z^2 \tag{2}$$

where χ, λ and μ are the shape characteristic quantities of the propellant, ψ is the combustible relative mass of the propellant, σ is the relative surface area of the combustible

powder, $Z = e/e_l$ represents the relative thickness, e is the arc thickness at any time and e_l is the starting arc thickness.

The 0-D combustion model based on Saint Robert's law is used to calculate the pressure of the gas inside the chamber, which is essential for obtaining the actuating force. The relationship between the burn rate, r_b, arc thickness, e, and pressure is as follows [29]:

$$r_b = \frac{de}{dt} = uP^n \tag{3}$$

where P is the pressure, n is the burn rate exponent and u is a constant determined by the chemical composition and initial temperature of the propellant.

In conclusion, the mass generation rate of the gas from the CPN particles is estimated as follows [30]:

$$\dot{m}_{gen} = \eta_g m_p \frac{d\psi}{dt} \tag{4}$$

where η_g is the mass fraction of gas in the combustion product of the propellant and m_p is the loading mass of the propellant.

The aforementioned combustion model can be used to calculate the pressure inside the chamber. Hence, the law of conservation of mass in a control volume of the combustion chamber is given by the following equation [31]:

$$d(\rho_g V)/dt = \dot{m}_{gen} \tag{5}$$

where ρ_g is the density of the propellant gas and V is the volume of the combustion chamber.

Equation (6) can be obtained from Equation (5):

$$\frac{d\rho_g}{dt} = \frac{\dot{m}_{gen} - \rho_g \dot{V}}{V} \tag{6}$$

where $\dot{V}$ is the rate of change of the volume of the combustion chamber, as given by the following equation:

$$\dot{V} = \dot{m}_{gen}/\rho_s - (1 - \eta_g)\dot{m}_{gen}/\rho_{cp} + A_{sle}v_{sle} + A_{piston}v_{piston} \tag{7}$$

where ρ_s is the density of the CPN particles and ρ_{cp} is the density of the condensed phase in the powder product.

The energy conservation relation of the internal gas can be expressed by Equation (8) [32]:

$$\frac{d(\rho_g V c_v T)}{dt} = \eta_p \dot{m}_{gen} c_p T_f - P(A_{sle}v_{sle} + A_{piston}v_{piston}) - \dot{Q}_{loss} \tag{8}$$

where η_p is the non-ideal gas correction factor, c_v and c_p are the specific heats of constant volume and pressure of the gas, respectively, T_f is the explosion temperature at constant pressure, A_{sle} and A_{piston} are the compression areas of the inner sleeve and piston, respectively, v_{sle} and v_{piston} are the separation speeds of the inner sleeve and piston, respectively, $\dot{Q}_{loss}$ is the heat dissipation rate and T is the temperature of the gas.

For the high-temperature and high-pressure gas in the separation nut, the ideal gas state equations are given by Equations (9) and (10) [33].

$$P(1 - \rho_g \alpha_g) = \rho_g RT \tag{9}$$

Here, α_g is the covolume and R is the gas constant.

$$R = c_v(k - 1) \tag{10}$$

Here, k is the specific heat ratio of the fuel gas.

Equations (6) and (8) are combined and the ideal gas state equations (Equations (9) and (10)) are used to derive the rate of change of the pressure.

$$\frac{dP}{dt} = \frac{\dot{m}_{gen}\left(\eta_p kRT_f + P\alpha_g\right) - P\dot{V} - (k-1)\left[P(A_{sle}v_{sle} + A_{piston}v_{piston}) + \dot{Q}_{loss}\right]}{(1 - \rho_g\alpha_g)V} \tag{11}$$

A simplified model of heat exchange between the propellant products and the outside through the cavity wall is established according to [34], and the heat dissipation rate can be estimated using Equation (12):

$$\dot{Q}_{loss} = hA_w(T_w - T) + \sigma_s A_w(\alpha_w T_w^4 - \xi T^4) \tag{12}$$

where h is a constant convective heat transfer coefficient, T_w is the temperature of the vessel wall, σ_s is the Stefan–Boltzmann constant, α_w is the absorption rate of the vessel wall, ξ is the net emissivity of the product and A_w is the instantaneous surface area of the vessel side wall in contact with the product.

The combustion parameters applied to this combustion model are listed in Table 1.

Table 1. Parameters for the analytical combustion model.

Parameter	Value	Parameter	Value
Burn rate exponent (n)	0.45	Fraction of gases in product (η_g)	0.095
Non-ideal gas correction factor (η_p)	0.9	Covolume (α_g)	0.663 dm^3 kg^{-1}
Specific heat ratio (k)	1.09	Starting arc thickness of CPN (e_l)	488.6 μm
Explosion temperature (T_p)	2691.85 K	Convective heat transfer coefficient (h)	1050 W·m^{-2}·K^{-1}
Shape characteristic parameter of CPN (χ)	3	Stefan–Boltzmann constant (σ_s)	5.67 × 10^{-8} W·m^{-2}·K^{-1}
Shape characteristic parameter of CPN (λ)	−1	Net emissivity of the product (ξ)	0.6
Shape characteristic parameter of CPN (μ)	1/3	Absorption rate of the vessel wall (α_w)	0.6
Density of the CPN particles (ρ_s)	1.3 g cm^{-3}		

2.1.2. Motion Modelling of the Separation Mechanism

The separation motion equations of the main separation mechanisms in the separation stage are established according to the different separation states of the separation nut.

(1)　Inner sleeve separation model

The force analysis of the inner sleeve is shown in Figure 3, and the separation equation of the inner sleeve is derived from Equations (13)–(15):

$$PA_{sle} > F_{shear} + F_{f,oring1} + F_{f,oring2} + F_{f,nut} \tag{13}$$

$$F_{f,nut} = \mu_{nut-sle}F_{N,nut} = \mu_{nut-sle}\frac{\left(PA_{piston} - F_{f,oring2}\right)(\tan\alpha + \tan\delta) + F_{pre}(\tan\gamma + \tan\delta)}{1 + \mu_{nut-sle}\tan\delta} \tag{14}$$

$$\dot{x}_{sle} = dx_{sle}/dt_1 = v_{sle} \tag{15}$$

where F_{shear} is the shear force of the shear pin, $F_{f,oring}$ is the friction force of the sealing ring, $F_{f,nut}$ is the friction force between the inner sleeve and nut flap, F_{pre} is the preload applied by the mounting bolt, $\mu_{nut-sle}$ is the friction coefficient between the inner sleeve and nut flap and t_1 is the separation time of the inner sleeve.

(2)　Piston separation model

A force analysis of the piston separation is shown in Figure 4. The separation equation of the piston in the axial direction is as follows:

$$m_{piston}a_{piston} = PA_{piston} - F_{f,oring2} - F_{nut-piston,ax} - F_{f,piston-nut}\sin\alpha \tag{16}$$

where m_{piston} is the mass of the piston, a_{piston} is the acceleration of the piston, $F_{nut-piston,ax}$ is the axial pressure between the nut flap and the piston, $F_{f,piston-nut}$ is the friction between the nut flap and the piston and α is the support angle between the piston and the nut flap.
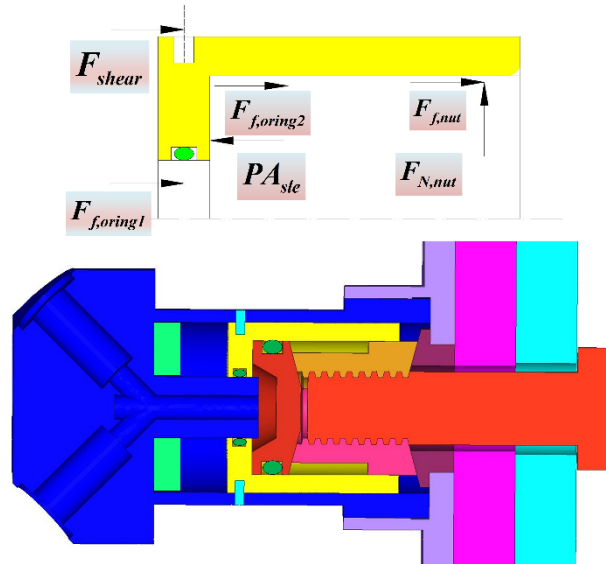
Figure 3. Force analysis of the inner sleeve.
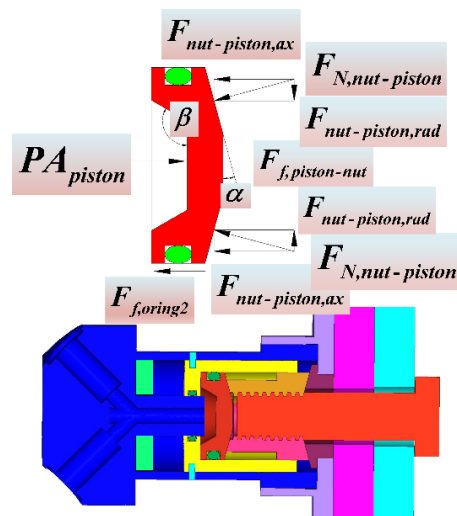
Figure 4. Force analysis of piston.

(3)   Nut flap separation model

When the inner sleeve releases the constraint on the nut flap, the latter begins to separate. A stress analysis of the nut flap is shown in Figure 5. The axial and radial separation equations of the nut flap are obtained using Equations (17) and (18).

$$\frac{d^2 x_{nut,ax}}{dt_2^2} = \frac{F_{nut-piston,ax} + F_{bolt,ax} - F_{end,ax} + F_{f,piston-nut}\sin\alpha + F_{f,bolt-nut}\sin\gamma - F_{f,end-nut}\sin\delta}{m_{nut}} \quad (17)$$

$$\frac{d^2 x_{nut,rad}}{dt_2^2} = \frac{F_{nut-piston,rad} + F_{bolt,rad} + F_{end,rad} - F_{f,piston-nut}\cos\alpha - F_{f,bolt-nut}\cos\gamma - F_{f,end-nut}\cos\delta}{m_{nut}} \quad (18)$$

where $x_{nut,ax}$ and $x_{nut,rad}$ are the axial and radial displacements of the nut flap, respectively, $F_{nut-piston,rad}$ is the radial pressure between the nut flap and the piston, $F_{bolt,ax}$ and $F_{bolt,rad}$ are the axial and radial pressures of the bolt, respectively, $F_{end,ax}$ and $F_{end,rad}$ are the axial

and radial pressures of the end cap, respectively, $F_{f,bolt-nut}$ is the friction between the bolt and nut flap, $F_{f,end-nut}$ is the friction between the end cap and the nut flap, γ is the half angle of the tooth profile of the nut flap, δ is the support angle between the nut flap and the end cap, m_{nut} is the mass of the nut flap and t_2 is the separation time of the nut flap.
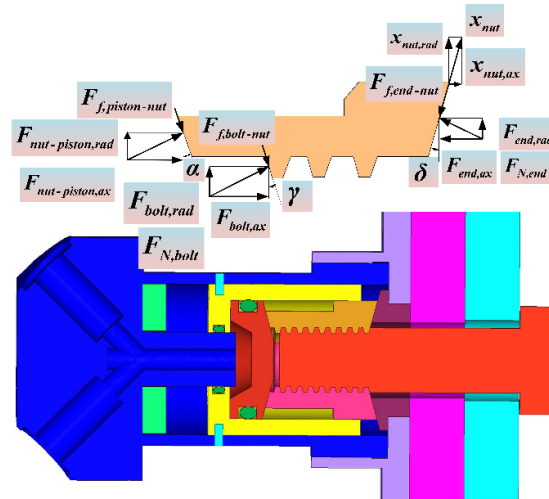
Figure 5. Force analysis of the nut flap.

In this study, the simulation model of the separation nut is calculated and analysed by using the MATLAB/Simulink. Simulink is a visual simulation tool based on block diagram design environment. It provides a large number of simulation design blocks, such as input/output, mathematical calculation, integral/differential, signal processing and other modules, which can avoid a large number of writing programs. Meanwhile, differential equation solvers such as ODE45, ODE23 and ODE113 are provided in Simulink, which provides convenience for solving many differential equations in the separation simulation model. The initial values of the parameters for the motion model of the separation nut are listed in Table 2.

Table 2. Initial values of motion parameters of the separation nut mechanism.

Parameter	Value	Parameter	Value
Initial volume (V)	1.10×10^{-6} m^3	Shear pin diameter (d)	1.5 mm
Inner sleeve quality (m_{sle})	0.06126 kg	Supporting angle between piston and nut flap (α)	15°
Compression area of inner sleeve (A_{sle})	3.17×10^{-4} m^2	Side angle of screw thread (γ)	15°
Piston quality (m_{piston})	13.74×10^{-3} kg	Supporting angle between end cap and nut flap (δ)	15°
Compression area of piston (A_{piston})	1.68×10^{-4} m^2	Nut flap quality (m_{nut})	9.57×10^{-3} kg
Preload (F_{pre})	12,000 N	Friction coefficient between inner sleeve and nut flap ($\mu_{nut-sle}$)	0.07

The pressure in the cavity and the motion curve of each mechanism are shown in Figure 6.

As shown in Figure 6, the shear pin is sheared at 0.26 ms under the action of high pressure, and the inner sleeve is started. At 4.45 ms, the inner sleeve moves by 5 mm, releasing the radial restraint on the nut flap. At the same time, the nut flap and piston are started. At 5.18 ms, the radial displacement of the nut flap reaches 1 mm, and the restraint on the bolt is released. Under the action of the preload, the bolt begins to separate from the separation nuts to realise separation, and the inner sleeve, piston and nut flap move

continuously. At 5.70 ms, the piston and nut flap move to the designed maximum stroke and stop moving. At 9.96 ms, the inner sleeve moves to the designed maximum stroke.
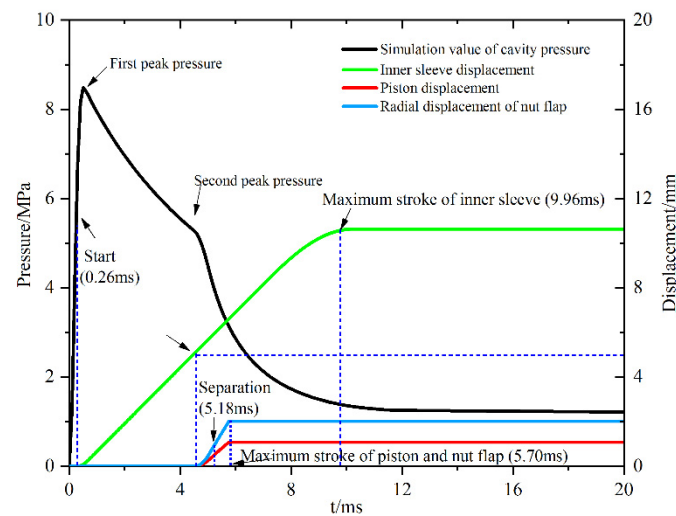
Figure 6. Simulated output curves of the separation nut.

To verify the simulation results of the motion of the separation nut mechanism, a pressure sensor is used to test the pressure of the separation chamber. The output pressure of the electric squib is measured at 15 MPa (5 mL). The selected sensors are listed in Table 3.

Table 3. Pressure sensor parameters.

Model	Type	Range/MPa	Linearity Error/%	Sensitivity/pC·MPa^{-1}	Working Temperature/°C	Resonant Frequency/kHz	Shock Resistance/g	Overload/MPa
KISTLER601A	Piezoelectric	25	±0.27	150	−196–200	150	10,000	50

To simulate the axial gravity-free state of the separation device of the inter-stage cabin and reduce the interference of the external environment on the sensor, the test plates (600 mm × 60 mm × 10 mm) are lifted by four flexible elastic ropes. The connecting plate is connected to the test plates to simulate the separation state. The test system is shown in Figure 7.

The separation process of the separation nut is evaluated by employing the separation test system of the separation nuts, and the key separation parameters, such as cavity pressure, are measured. The test curve is shown in Figure 8.

To analyse the pressure change process more intuitively, the values of the pressure and time of the first peak and second peak, as shown in the curve of Figure 6, are compared and presented in Table 4. The relative errors of the key pressure parameters are 1.30%, 1.96%, 3.48% and 2.97%, which are all less than 5%. This shows that the simulation model can accurately predict the variation law of the pressure in the cavity during the action of the separation nut and accurately describe the motion law of the separation nut mechanism.

Table 4. Simulation values and test values of the unlocking pressure in the cavity of the separation nut.

	First Peak Pressure/MPa	First Peak Pressure Time/ms	Second Peak Pressure/MPa	Second Peak Pressure Time/ms
Experimental value	8.47	0.51	5.46	4.38
Simulation value	8.58	0.52	5.27	4.51
Relative error	1.30%	1.96%	3.48%	2.97%
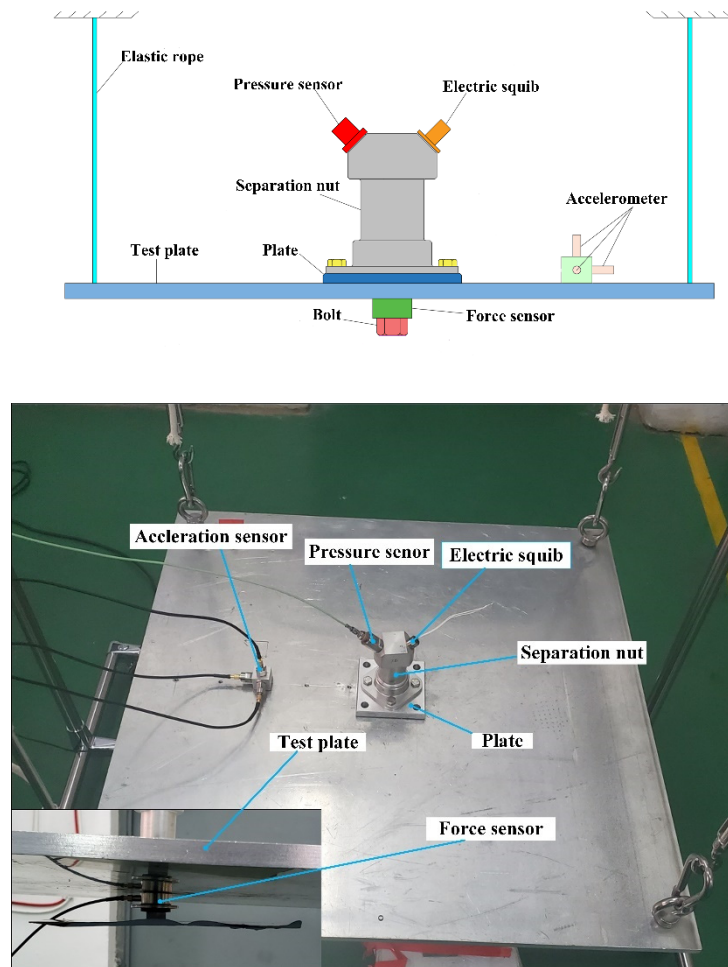
Figure 7. Separation test system for the separation nut.
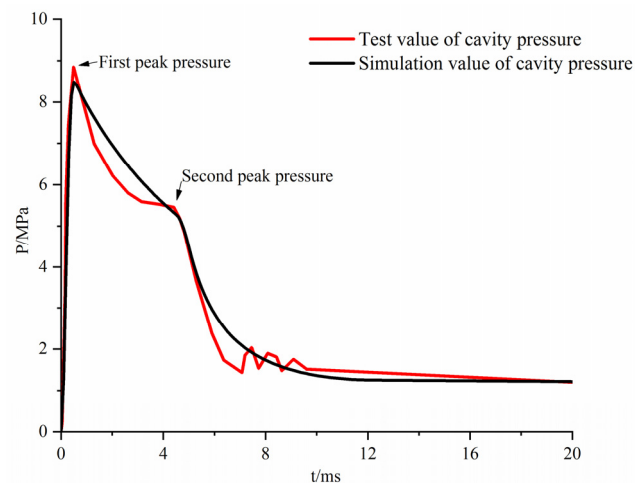
Figure 8. Comparison curve of simulated and tested unlocking pressures in the cavity of the separation nut.

3. Separation Reliability Modelling of the Separation Nut Mechanism

3.1. Separation Limit State Function of the Separation Nut Mechanism

To successfully complete the separation function of the separation nut, the movement of its mechanism must reach the desired size. Therefore, according to the separation

law of the separation nut mechanism and the stress-strength model [35], the limit state functions, $g_1(x)$ and $g_2(x)$, for the separation of the inner sleeve and nut flap, respectively, are expressed as Equation (19).

$$\begin{cases} g_1(x_{sle}) = d(x_{sle}) - d_{unlock-sle} \\ g_2(x_{nut}) = d(x_{nut}) - d_{unlock-nut} \end{cases} \tag{19}$$

Here, x_{sle} and x_{nut} are the vectors of random variables such as external load, material property, structural dimension and machining error that affect the movement of the inner sleeve and nut flap, respectively. $d(x_{sle})$ is the displacement function of the inner sleeve. $d_{unlock-sle}$ is the critical displacement of the inner sleeve to release the constraint of the nut flap and is 5 mm according to the design requirements. $d(x_{nut})$ is the displacement function of the nut flap, and $d_{unlock-nut}$ is the critical radial displacement of the nut flap to release the constraint of the bolt and has a value of 2 mm.

According to reliability theory [36], the failure probability model is as follows:

$$P_f = P(g(x) < 0) \tag{20}$$

where P_f is the failure probability, and when $g(x) > 0$, the mechanism of separation nut can be separated reliably. When $g(x) < 0$, the mechanism of the separation nut is not reliably separated. At $g(x) = 0$, the limit state occurs. Therefore, the reliability model is as follows:

$$R = 1 - P_f = P(g(x) \geq 0) \tag{21}$$

3.2. Kriging Surrogate Model

Because $d(x)$ is the displacement response value of the inner sleeve or nut flap obtained from the separation simulation model of the separating nut mechanism, $d(x)$ is an implicit function relative to x. Therefore, function $g(x)$ is also an implicit function in mathematics. To solve the problem of the nonlinear implicit function and improve the calculation efficiency of the reliability analysis, the Kriging surrogate model is used to display the nonlinear implicit function. According to the Kriging theory [37], the output function, $\hat{d}(x)$, and random variable, x, are related as follows:

$$\hat{d}(x) = f^T(x) + \varepsilon(x) \tag{22}$$

where $\beta = \{\beta_1, \beta_2, \dots, \beta_n\}^T$ is the regression coefficient, $f(x) = \{f_1(x), f_2(x), \dots, f_n(x)\}^T$ is the polynomial function of variable x and n is the number of polynomial functions. A global approximation is simulated in the design space. $\varepsilon(x)$ is a random correction process that provides local approximation and obeys the normal distribution, $N(0, \sigma^2)$, and the covariance is nonzero. Therefore, the covariance matrix can be expressed as [38]

$$Cov[\varepsilon(x_i), \varepsilon(x_j)] = \sigma^2 R(x_i, x_j) \tag{23}$$

where $R[(x_i, x_j)i, j = 1, 2, \cdots, m]$ is the spatial correlation function of the sum of any two sample points, which is the component of the correlation matrix, $\boldsymbol{R}$, and m is the number of experimental design samples. This plays a decisive role in the accuracy of the simulation. A Gaussian type correlation function is adopted and expressed as follows:

$$R(x_i, x_j) = exp(-\sum_{k=1}^{m} \theta_k \left| x_k^{(i)} - x_k^{(j)} \right|^2) \tag{24}$$

where $\theta_k (k = 1, 2, \cdots, m)$ is an unknown related parameter.

According to the Kriging theory, the estimated value of the response at prediction point x can be expressed as Equation (25).

$$\hat{d}(x) = f^T(x)\hat{\beta} + r^T(x)R^{-1}(d - F\hat{\beta}) \tag{25}$$

where $\hat{\beta}$ is the estimated value of β, d is the column vector composed of the response value of the experimental design sample data, that is, $d = [d(x_1), d(x_2), \ldots, d(x_m)]^T$, F is the $m \times n$ order matrix composed of the regression model at m sample points and $r(x)$ is the correlation function vector between the experimental data sample points and the prediction points and can be expressed as Equation (26).

$$r^T(x) = \left\{ R\left(x, x^{(1)}\right), R\left(x, x^{(2)}\right), \ldots, R\left(x, x^{(m)}\right) \right\} \tag{26}$$

$\hat{\beta}$ and variance estimate $\hat{\sigma}^2$ are given as Equation (27).

$$\begin{aligned} \hat{\beta} &= (F^T R^{-1} F)^{-1} F^T R^{-1} g \\ \hat{\sigma}^2 &= \tfrac{1}{m} (g - F\hat{\beta})^T R^{-1} (g - F\hat{\beta}) \end{aligned} \tag{27}$$

The relevant parameter, $\theta = \{\theta_1, \theta_2, \cdots, \theta_m\}^T$, is obtained by calculating the maximum value of the maximum likelihood estimation, as shown in Equation (28).

$$\max F(\theta) = -\frac{m \ln(\hat{\sigma}^2) + \ln|R|}{2}, \theta_k \geq 0 (k = 1, 2, \cdots, m) \tag{28}$$

Equations (19) and (22) are combined to obtain the display function given by Equation (29):

$$\begin{cases} \hat{g}_1(x_{sle}) = \hat{d}(x_{sle}) - d_{unlock-sle} \\ \hat{g}_2(x_{nut}) = \hat{d}(x_{nut}) - d_{unlock-nut} \end{cases} \tag{29}$$

3.3. Reliability and Sensitivity Analysis

When Equation (29) is used to calculate the reliability, the reliability analysis model can be expressed as

$$R = P(\hat{g}(x) \geq 0) = \int\limits_{\hat{g}(x) \geq 0} f(x) dx \tag{30}$$

where $f(x)$ is the joint probability density function of the random vector x.

The reliability calculations based on Equation (30) require the Monte Carlo simulation (MCS) [39] and first-order reliability method (FORM) [40] for solving the failure probability.

According to [41], the formula for calculating parameter sensitivity is defined as follows:

$$S_\varphi = \lambda \frac{\partial \beta}{\partial \varphi} = \lambda \left[\frac{\partial u}{\partial \varphi} \right]^T \frac{\partial \beta}{\partial u} \tag{31}$$

where β is the reliability index according to [42], that is, $R = \phi(\beta)$. φ can be the mean values or standard deviations of the random variables, x and $\lambda = [\lambda_{ij}]_{n \times n}$, where λ_{ij} represents the standard deviation of the ith random variable when $i = j$, and its value is 0 when $i \neq j$. u is an independent standard normal random vector, given by Equation (32).

$$u = L_0^{-1} y \tag{32}$$

where y is the random variable vector of the equivalent standard normal transformation of x, obtained based on the Nataf transformation [43]. L_0 is the lower triangular matrix obtained by the Choleskey decomposition of the correlation coefficient matrix of y.

4. Implementation of the Reliability Simulation

According to the aforementioned reliability analysis method, the separation reliability simulation of the separation nut mechanism includes the following steps.

Step 1. Enter the random variable, x, and its distribution type, as shown in Tables 5 and 6.

Table 5. Key design parameters for the separation of the inner sleeve.

Symbol	Mean	Std.	Distribution Type	Symbol	Mean	Std.	Distribution Type
d (mm)	1.5	0.00667	Normal	γ (°)	15	0.03	Normal
A_{sle} (mm^2)	317	0.715	Normal	n	0.45	0.01	Normal
F_{pre} (N)	12,000	348	Normal	ρ (g/cm^3)	1.3	0.074	Normal
α (°)	15	0.03	Normal				

Table 6. Key design parameters for the separation of the nut flap.

Symbol	Mean	Std.	Distribution Type	Symbol	Mean	Std.	Distribution Type
A_{piston} (mm^2)	168	0.648	Normal	γ (°)	15	0.03	Normal
F_{pre} (N)	12,000	384	Normal	δ (°)	15	0.03	Normal
n	0.45	0.01	Normal	ρ (g/cm^3)	1.3	0.074	Normal
α (°)	15	0.03	Normal				

Step 2. Because there are more than five random variables in the experiment, m groups of sample data x are obtained by applying a three-level full-factor design [44] to reduce the number of experiments. In this case, the range of input variables is $[\mu - 3\,\sigma, \mu + 3\,\sigma]$, where μ and σ are the mean and standard deviation, respectively, of the random variables. After obtaining m group samples through experimental optimisation design, the samples are input into the separation simulation model of separation nut mechanism established by MATLAB to obtain the displacement value $d(x)$ of mechanism movement. Among them, the simulation model is run in batch mode.

Step 3. The Kriging model, $\hat{g}(x)$, is fitted based on m groups of the sample data.

Step 4. The reliability and sensitivity are analysed based on the Kriging model, $\hat{g}(x)$. The simulation flow chart is shown in Figure 9.
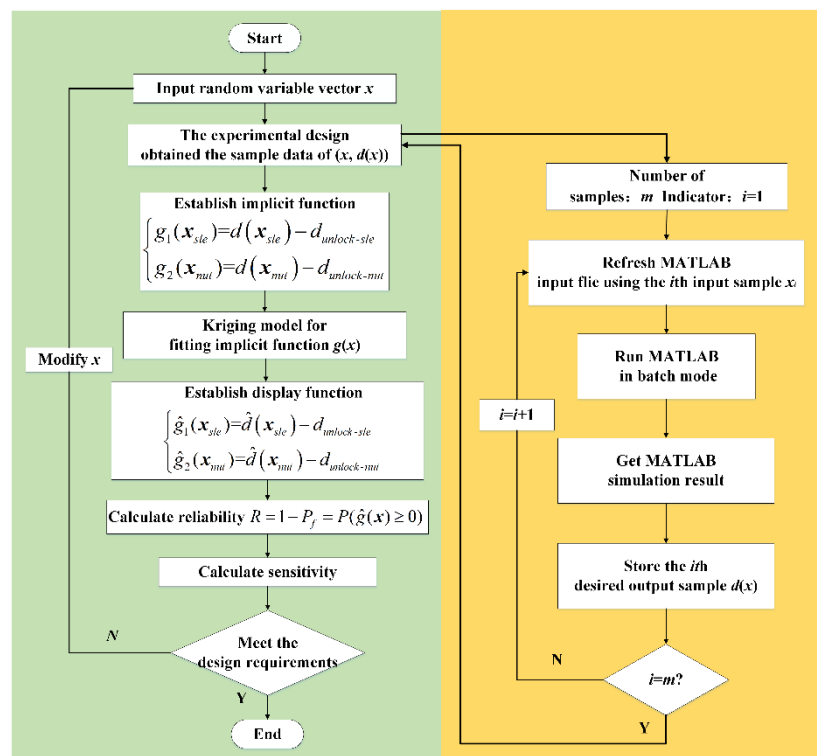
Figure 9. Simulation flow chart of the separation reliability of the separation nut mechanism.

The simulation workflows of the inner sleeve and nut flap are constructed by applying the aforementioned steps of the reliability analysis, as shown in Figures 10 and 11. The

arrows in the figure represent the running order of the tasks. The details of the nodes in the simulation workflow are listed in Table 7.
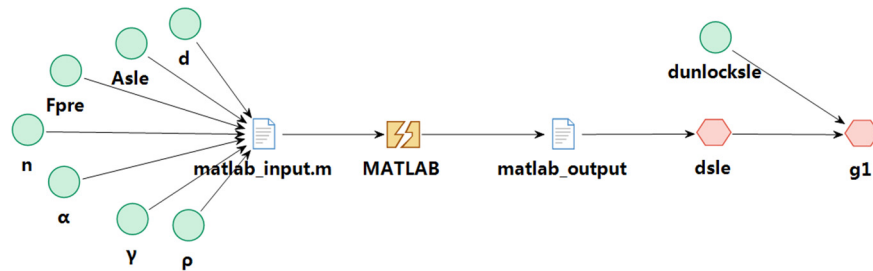
Figure 10. Simulation workflow of the separation reliability of the inner sleeve.
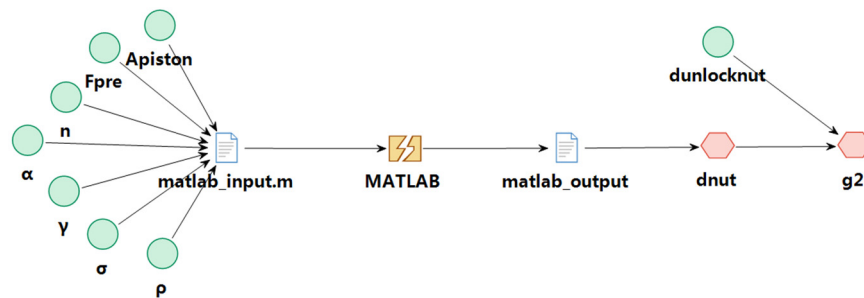
Figure 11. Simulation workflow of the separation reliability of the nut flap.

Table 7. Nodes in the simulation workflow.

Name/Inner Sleeve	Type	Name/Nut Flap	Type
d	Input variable	A_{piston}	Input variable
A_{sle}	Input variable	F_{pre}	Input variable
F_{pre}	Input variable	n	Input variable
n	Input variable	α	Input variable
α	Input variable	γ	Input variable
γ	Input variable	δ	Input variable
ρ	Input variable	ρ	Input variable
$d_{unlock\text{-}sle}$	Input variable	$d_{unlock\text{-}nut}$	Input variable
MATLAB_input.m	MATLAB input script file	MATLAB_input.m	MATLAB input script file
MATLAB_output	MATLAB output file	MATLAB_output	MATLAB output file
MATLAB	MATLAB execution commands	MATLAB	MATLAB execution commands
d_{sle}	Output variable	d_{nut}	Output variable
$g1$	Function of inner sleeve separation	$g2$	Function of nut flap separation

5. Reliability and Sensitivity Analysis Results

According to the separation reliability simulation program of the separation nut mechanism described in Section 4, 2187 sets of sample data of the input variable, x, and output displacement function value, $d(x)$, are obtained. The Kriging response surface model of some random variables, x, is shown in Figure 12.

Based on Equation (21), it is impractical to use the MCS method to analyse reliability, and it takes approximately 10^6 times to evaluate the function [45], which is time-consuming (an average simulation time of a single cycle 1 min on a 2.6 GHz PC). Therefore, in this study, the reliability is analysed based on the Kriging surrogate model of Equation (30), and the correctness of the reliability analysis results is verified by using the importance sampling method [46]. The reliability results of different mechanism separations analysed by combining different methods with the Kriging surrogate model are presented in Tables 8 and 9.

(a)

(b)
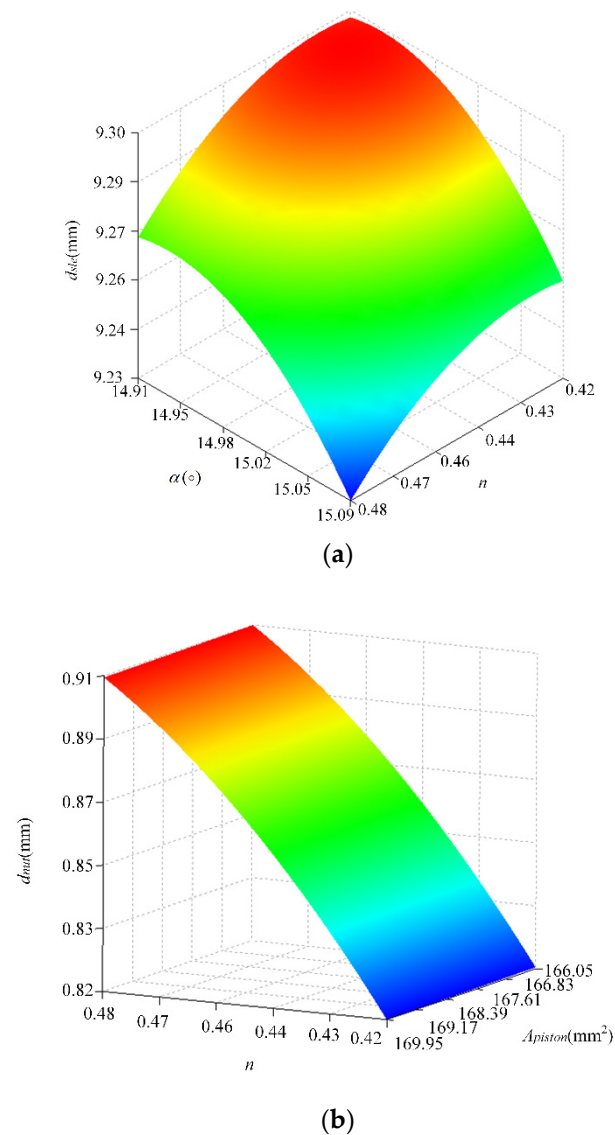
Figure 12. Response surface of the Kriging model. (**a**) $d_{sle} \sim (\alpha, n)$. (**b**) $d_{nut} \sim (A_{piston}, n)$.

Table 8. Results for the separation reliability of the inner sleeve.

Method	R_{sle}	β
Kriging Model + FORM	0.99997	8.3284
Kriging Model + MCS	0.99998	8.3556
Importance sampling (10^4 samples)	0.99994	8.3748

Table 9. Results for the separation reliability of the nut flap.

Method	R_{nut}	β
Kriging Model + FORM	0.99668	1.4999
Kriging Model + MCS	0.99846	1.4234
Importance sampling (10^4 samples)	0.99546	1.4137

Because the mechanical motion of the separation nut belongs to the series model, the separation reliability of the separation nut mechanism is calculated by using the series calculation method, as shown in Table 10. The relative errors of the Kriging Model+FORM and Kriging Model+MCS are 0.1% and 0.3%, respectively. Therefore, the simulation method is suitable for the functional reliability analysis of separation nuts.

Table 10. Functional reliability analysis results of separation nuts.

Method	R	Relative Error (%)
Kriging Model + FORM	0.99665	0.125
Kriging Model + MCS	0.99844	0.305
Importance sampling(10^4 samples)	0.99540	NA

The random variable sensitivity analysis results of the inner sleeve separation and nut flap separation described by Equation (31) are presented in Figures 13 and 14. Figure 13 shows the dimensionless reliability sensitivities of the inner sleeve separation. Among these, n and γ positively affect the results of the mean sensitivity analysis; that is, increasing the mean value of these parameters improves the reliability of the inner sleeve motion. Parameters d, A_{sle}, F_{pre}, α and ρ have a negative effect on the mean sensitivity; in other words, reducing the mean value of its parameters improves the separation reliability of the inner sleeve. The sensitivity results of the standard deviation indicate that reducing the standard deviation of each variable aids in improving the motion reliability of the inner sleeve. Similarly, Figure 14 shows the dimensionless reliability sensitivities of the separation of the nut flap. The mean sensitivities of n and γ are positive value, so the reliability increases as the mean of n and γ increase. The mean sensitivities of F_{pre}, A_{piston}, α, δ and ρ are negative values, so the reliability decreases as the mean of F_{pre}, A_{piston}, α, δ and ρ increase. The standard-deviation sensitivities of n, F_{pre}, A_{piston}, α, δ, ρ and γ are negative values, so the reliability decreases as the standard deviations of n, F_{pre}, A_{piston}, α, δ, ρ and γ increase.
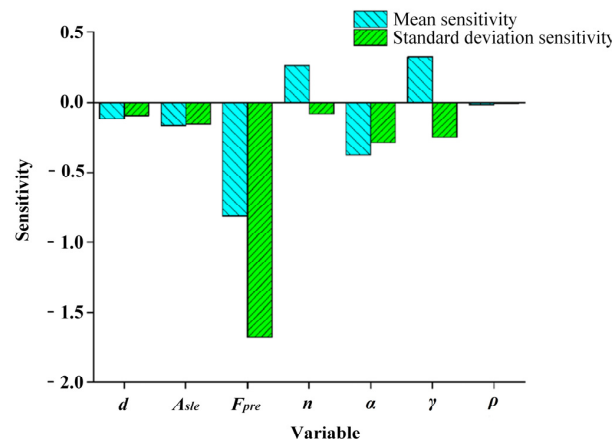
Figure 13. Sensitivity results for the inner sleeve separation.
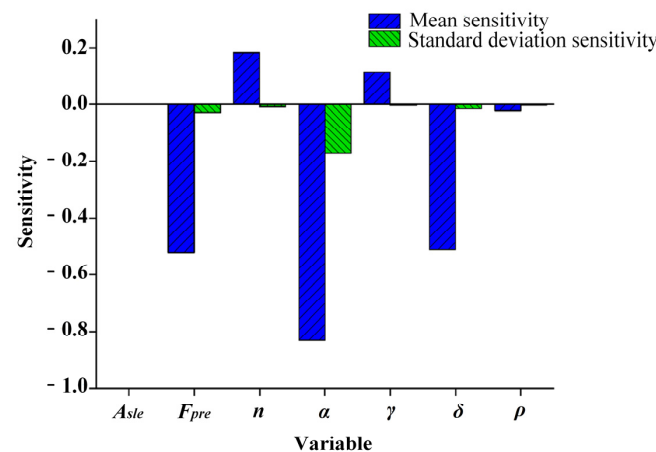
Figure 14. Sensitivity results for the nut flap separation.

6. Conclusions

Based on the combination of the separating simulation model of the separation nut mechanism and the Kriging model, a functional reliability simulation method for a low-shock separation nut was proposed for the first time, and its effectiveness was verified.

(1) A simulation model of the mechanism separation was established according to the motion law of the separation nut mechanism, and the accuracy of the simulation model was verified experimentally.

(2) The implicit function of different separation mechanisms of the separation nut was established by selecting random variables such as the working load, geometric size and propellant combustion parameters.

(3) Finally, a separation reliability simulation model of the low-shock separation nut mechanism was established. The importance order of random variables was quantified by conducting a sensitivity analysis, providing valuable ideas for the reliability and optimisation designs of low-shock separation nuts. During the process of inner sleeve separation, F_{pre}, α and γ were the main factors affecting the reliability of the inner sleeve separation, followed by n, d, A_{sle} and ρ. During nut flap separation, α, F_{pre} and δ were the main factors affecting the reliability of nut petal separation, followed by n, γ, ρ and A_{piston}. The reliability of products can be optimised by adjusting the magnitudes of these design values, and their consistency should be maintained during the design process.

Further research needs to be considered concerning the reliability of separation nut including the effect of parameter correlation on reliability and separation mechanisms leading to time-varying reliability.

References

1. Benedetti, M.D.; Garofalo, G.; Zumpano, M.; Barboni, R. On the damping effect due to bolted junctions in space structures subjected to pyro-shock. *Acta Astronaut.* **2007**, *60*, 947–956. [CrossRef]
2. Bement, L.J.; Schimmel, M.L. *A Manual for Pyrotechnic Design, Development and Qualification*; Report No. NASA TM-110172; NASA Langley Research Center: Hampton, VA, USA, 1995.
3. Brauer, K.O. *Handbook of Pyrotechnics*; Chemical Publishing Co.: New York, NY, USA, 1974.
4. Lee, J.; Hwang, D.H.; Jang, J.K.; Kim, D.J.; Lee, Y.; Lee, J.R.; Han, J.H. Pyroshock prediction of ridge-cut explosive bolts using hydrocodes. *Shock. Vib.* **2016**, *2016*, 14. [CrossRef]
5. Wang, X.; Qin, Z.; Ding, J.; Chu, F. Finite element modeling and pyroshock response analysis of separation nuts. *Aerosp. Sci. Technol.* **2017**, *68*, 380–390. [CrossRef]
6. Zhao, H.; Liu, W.; Ding, J.; Sun, Y.; Li, X.; Liu, Y. Numerical study on separation shock characteristics of pyrotechnic separation nuts. *Acta Astronaut.* **2018**, *151*, 893–903. [CrossRef]
7. Woo, J.; Cha, S.W.; Cho, J.Y.; Kim, J.H.; Roh, T.; Jang, S.G.; Lee, H.-N.; Yang, H.W. Prediction of pyroshock-reduced separation nut behaviors. *J. Propuls. Power* **2018**, *34*, 1240–1255. [CrossRef]
8. Zhang, H.; Liu, T.; Li, C.; Xiang, S.; Zhang, Q. Numerical simulation of pyrotechnic shock environment concerning pyroshock separation nuts of spacecraft. *Spacecr. Environ.* **2014**, *31*, 363–368.
9. Lee, J.; Han, J.-H.; Lee, Y.; Lee, H. A Parametric Study of Ridge-cut Explosive Bolts using Hydrocodes. *Int. J. Aeronaut. Space Sci.* **2015**, *16*, 50–63. [CrossRef]
10. Lee, J.; Han, J.-H.; Lee, Y.; Lee, H. Separation characteristics study of ridge-cut explosive bolts. *Aerosp. Sci. Technol.* **2014**, *39*, 153–168. [CrossRef]

11. Huang, X.; Chen, J.; Zhu, H. Assessing small failure probabilities by AK–SS: An active learning method combining Kriging and Subset Simulation. *Struct. Saf.* **2016**, *59*, 86–95. [CrossRef]
12. Bucher, C.; Bourgund, U. A fast and efficient response surface approach for structural reliability problems. *Struct. Saf.* **1990**, *7*, 57–66. [CrossRef]
13. Sofi, A.; Muscolino, G.; Giunta, F. Propagation of uncertain structural properties described by imprecise Probability Density Functions via response surface method. *Probabilistic Eng. Mech.* **2020**, *60*, 103020. [CrossRef]
14. Dai, H.; Zhang, H.; Wang, W.; Xue, G. Structural reliability assessment by local approximation of limit state functions using adaptive Markov chain simulation and support vector regression. *Comput. Aided Civ. Inf.* **2012**, *27*, 676–686. [CrossRef]
15. Xiao, N.; Yuan, K.; Zhou, C. Adaptive kriging-based efficient reliability method for structural systems with multiple failure modes and mixed variables. *Comput. Methods Appl. Mech. Eng.* **2020**, *359*, 112–649. [CrossRef]
16. Hurtado, J.E.; Alvarez, D.A. Neural-network-based reliability analysis: A comparative study. *Comput. Methods Appl. Mech. Eng.* **2001**, *191*, 113–132. [CrossRef]
17. Gong, Q.; Zhang, J.; Tan, C.; Wang, C. Neural Networks Combined with Importance Sampling Techniques for Reliability Evaluation of Explosive Initiating Device. *Chin. J. Aeronaut.* **2012**, *25*, 208–215. [CrossRef]
18. Bdour, T.; Guiffaut, C.; Reineix, A. Use of adaptive kriging metamodeling in reliability analysis of radiated susceptibility in coaxial shielded cables. *IEEE Trans. Electromagn. Compat.* **2016**, *58*, 95–102. [CrossRef]
19. Yun, W.Y.; Lu, Z.Z.; Jiang, X. AK-SYSi: An improved adaptive Kriging model for system reliability analysis with multiple failure modes by refined U learning function. *Struct. Multidiscip. Optim.* **2019**, *59*, 263–278. [CrossRef]
20. Hristov, P.O.; DiazDelaO, F.A.; Farooq, U.; Kubiak, K.J. Adaptive Gaussian process emulators for efficient reliability analysis. *Appl. Math. Model.* **2019**, *71*, 138–151. [CrossRef]
21. Allaix, D.L.; Carbone, V.I. An improvement of the response surface method. *Struct. Saf.* **2011**, *33*, 165–172. [CrossRef]
22. Zhang, M.-D.; Dai, H.-F.; Hu, B.-Q.; Chen, Q. Robust adaptive UKF based on SVR for inertial based integrated navigation. *Def. Technol.* **2020**, *16*, 846–855. [CrossRef]
23. Echard, B.; Gayton, N.; Lemaire, M. AK-MCS: An active learning reliability method combining Kriging and Monte Carlo Simulation. *Struct. Saf.* **2011**, *33*, 145–154. [CrossRef]
24. Zheng, P.J.; Wang, C.M.; Zong, Z.H.; Wang, L.Q. A new active learning method based on the learning function U of the AK-MCS reliability analysis method. *Eng. Struct.* **2017**, *148*, 185–194.
25. Chen, W.D.; Xu, C.L.; Shi, Y.Q.; Ma, J.X.; Lu, S.Z. A hybrid Kriging-based reliability method for small failure probabilities. *Reliab. Eng. Syst. Saf.* **2019**, *189*, 31–41. [CrossRef]
26. Keshtegar, B.; Nguyen-Thoi, T.; Truong, T.T.; Zhu, S.-P. Optimization of buckling load for laminated composite plates using adaptive Kriging-improved PSO: A novel hybrid intelligent method. *Def. Technol.* **2021**, *17*, 85–99. [CrossRef]
27. Zhang, J.; Xiao, M.; Gao, L. An active learning reliability method combining Kriging constructed with exploration and exploitation of failure region and subset simulation. *Reliab. Eng. Syst. Saf.* **2019**, *188*, 90–102. [CrossRef]
28. Jin, Z.M. *Interior Ballistics of Guns Beijing*; Beijing Institute of Technology Press: Beijing, China, 2004.
29. Kubota, N. *Propellants and Explosives: Thermochemical Aspects of Combustion*; John Wiley & Sons: New York, NY, USA, 2015.
30. Jang, S.-G.; Lee, H.-N.; Oh, J.-Y. Performance modeling of a pyrotechnically actuated pin puller. *Int. J. Aeronaut. Space Sci.* **2014**, *15*, 102–111. [CrossRef]
31. Han, D.-H.; Sung, H.-G.; Jang, S.-G.; Ryu, B.-T. Parametric analysis and design optimization of a pyrotechnically actuated device. *Int. J. Aeronaut. Space Sci.* **2016**, *17*, 409–422. [CrossRef]
32. Hwang, D.; Han, J.; Lee, J.; Lee, Y.J.; Kim, D. A mathematical model for the separation behavior of a split type low-shock separation bolt. *Acta Astronaut.* **2019**, *164*, 393–406. [CrossRef]
33. Zhang, X.; Yan, X.; Yang, Q. Design and experimental validation of compact, quick-response shape memory alloy separation device. *J. Mech. Des.* **2013**, *136*, 011009.1–011009.9. [CrossRef]
34. Gonthier, K.A.; Powers, J.M. Formulation, Predictions, and Sensitivity Analysis of a Pyrotechnically Actuated Pin Puller Model. *J. Propuls. Power* **1994**, *10*, 501–507. [CrossRef]
35. Liu, Y.; Shi, Y.; Bai, X.; Liu, B. Stress–strength reliability analysis of multi-state system based on generalized survival signature. *J. Comput. Appl. Math.* **2018**, *342*, 274–291. [CrossRef]
36. Ditlevsen, O.; Madsen, H.O. *Structural Reliability Methods*; John Wiley & Sons Ltd.: West Sussex, UK, 2007.
37. Lophaven, S.; Nielsen, H.; SØndergaard, J. *DACE a Matlab Kriging Toolbox*; Technical University of Denmark: Copenhagen, Denmark, 2002.
38. Cadini, F.; Santos, F.; Zio, E. An improved adaptive kriging-based importance technique for sampling multiple failure regions of low probability. *Reliab. Eng. Syst. Saf.* **2014**, *131*, 109–117. [CrossRef]
39. Metropolis, N.; Ulam, S. The Monte Carlo method. *J. Am. Stat. Assoc.* **1949**, *44*, 335–341. [CrossRef] [PubMed]
40. Hasofer, A.M.; Lind, N.C. An exact and invariant first order reliability format. *J. Eng. Mech. ASCE* **1974**, *100*, 111–121.
41. Tan, X.; Shen, M.; Juang, C.H.; Zhang, Y. Modified robust geotechnical design approach based on the sensitivity of reliability index. *Probabilistic Eng. Mech.* **2020**, *60*, 103049.1–103049.5. [CrossRef]
42. Cornell, C.A. A probability-based structural code. *J. Am. Concr. Inst.* **1969**, *66*, 974–985.
43. Der Kiureghian, A.; Liu, P.L. Structural reliability under incomplete probability information. *ASCE J. Eng. Mech.* **1986**, *112*, 85–104. [CrossRef]

44. Cheng, S.H.; Miao, J.M.; Wu, S.H. Investigating the effects of operational factors on PEMFC performance based on CFD simulations using a three-level full-factorial design. *Pergamon* **2012**, *39*, 250–260. [CrossRef]
45. Harbitz, A. An efficient sampling method for probability of failure calculation. *Struct. Saf.* **1986**, *3*, 109–115. [CrossRef]
46. Au, S.K.; Beck, J.L. Importance sampling in high dimensions. *Struct. Saf.* **2002**, *25*, 139–163. [CrossRef]